Supporting Information

Defect Regulating of Few-layer Antimonene from Acid-assisted Exfoliation for Enhanced Electrocatalytic Nitrogen Fixation

Shihai Cao[a,b1], Yuntong Sun[c1], Shiying Guo[d], Zichang Guo[a], Yanchao Feng[a], Sheng Chen[c], Huan Chen[a*], Shengli Zhang[d*], and Fang Jiang[a*]

[a] *Key Laboratory of Jiangsu Province for Chemical Pollution Control and Resources Reuse, School of Environmental and Biological Engineering, Nanjing University of Science and Technology, Nanjing 210094, Jiangsu, China*

[b] *College of Environmental Engineering, Nanjing Institute of Technology, Nanjing 211167, Jiangsu, China*

[c] *Key Laboratory for Soft Chemistry and Functional Materials, School of Chemical Engineering, Nanjing University of Science and Technology, Nanjing 210094, Jiangsu, China*

[d] *Institute of Optoelectronics & Nanomaterials, College of Materials Science and Engineering, Nanjing University of Science and Technology, Nanjing 210094, Jiangsu, China*

*E-mail: hchen404@njust.edu.cn (H. Chen), zhangslvip@njust.edu.cn (S. Zhang) fjiang@njust.edu.cn (F. Jiang)

[1]*S.C. and Y.S. contributed equally to this paper*

Experimental Procedures

Materials and Methods

Chemicals

Bulk antimony (Sb) powders, sodium hypochlorite (available chlorine 6-14%) and p-aminobenzaldehyde were purchased from Aladdin. Sodium sulphate (Na_2SO_4) was purchased from Energy Chemical. Concentrated sulfuric acid (H_2SO_4), hydrochloric acid (HCl), hydrazine sulfate, potassium sodium tartrate and sodium hydroxide were purchased from Sinopharm Chemical Reagent Co., Ltd. Ethanol was purchased from Nanjing Chemical Reagent Co., Ltd. Sodium salicylate and sodium nitroferricyanide were purchased from Chengdu Cologne Chemicals Co., Ltd. Ammonium chloride was purchased from Tianjin Kemiou Chemical Reagent Co., Ltd. Nafion (D520, 5%) was purchased from E.I. du Pont de Nemours and Company. Dimethyl sulfoxide solution (DMSO) was purchased from Sigma-Aldrich. All of the chemicals were used as received without further purification.

Characterization

Inductively coupled plasma (ICP) emission spectrometer data was measured on Agilent ICP-OES 720. The dynamic light scattering (DLS) was performed using Mastersizer 2000. Powder X-ray diffraction (XRD) patterns were recorded on a Bruker D8 multipurpose XRD system. Raman spectra of as-prepared samples were recorded on a Horiba Jobin Yvon Aramis raman microscopy with laser excitation of 532 nm. X-ray photoelectron spectroscopy (XPS) was performed on a Themo ESCALAB 250XI instrument with binding energies reference to adventitious carbon

at 284.6 eV. The morphology and structure of the samples were characterized by transmission electron microscopy (TEM, JEOL JEM-200CX), aberration-corrected high-resolution transmission electron microscope (FEI Titan 80-300), scanning electron microscope (SEM, HITACH S-3400N II) and atomic force microscopy (AFM, Bruker Veeco Multimode 8). Brunauer-Emmett-Teller (BET) method were used to determine the specific surface areas of the materials with a Micrometric ASAP 2000 Plus system. Electron paramagnetic resonance (EPR) spectra were conducted on a Bruker A300 EPR Spectrometer operating at room temperature and 1,1-Diphenyl-2-picrylhydrazyl (DPPH) is used as the standard to make a content result. ^{1}H NMR spectra were collected on a superconducting-magnet NMR spectrometer (Bruker AVANCE III HD 500 MHz).

Determination of NH_3

When NRR performed in 0.1 M Na_2SO_4 solution, the concentration of produced NH_3 was detected by Indophenol method.[1] We prepared 0, 0.1, 0.2, 0.4, 0.6, 0.8 and 1.0 μg mL^{-1} standard solutions. Specifically, 5.0 g sodium salicylate and 5.0 g sodium potassium tartrate were dissolved in 100 mL 1.0 M NaOH as a chromogenic reagent. The oxidizing solution is prepared by dissolving 3.5 mL of sodium hypochlorite (available chlorine 6-14 %) in 100 mL of ultrapure water. 0.5 g of sodium nitroferricyanide was added into 50 mL of ultrapure water as catalysing reagent. When NRR performed in 0.1 M Na_2SO_4 solution, 2.0 mL of standard solutions or sample solution were mixed with 2 mL of chromogenic reagent, 1.0 mL of oxidizing solution and 200 μL of catalysing reagent. After shaking and standing for 1.0 hour,

the solution was measuredd by UV-vis spectrophotometer at a wavelength of 655 nm, and the calibration curve about liner relation between the absorbance value with NH_3 concentration was obtained.

Determination of hydrazine

The hydrazine that may be formed in the electrolyte during the reaction was detected by the method of Watt and Chrisp.[2] A series of $N_2H_4 \cdot H_2SO_4$ standard solution with the concentrations of 0, 0.1, 0.2, 0.3, 0.4, 0.5 and 0.6 μg mL^{-1} in 0.12 M HCl were carefully prepared. We add 0.2 g p-aminobenzaldehyde to 10 mL of ethanol and 1.0 mL of concentrated hydrochloric acid mixed solution to prepare chromogenic reagent. 2.0 mL reacted electrolyte is mixed with 5 mL chromogenic reagent in the dark for 20 min and then measured the absorbance at 458 nm.

$^{15}N_2$ isotope labeling experiments

An isotopic labelling experiment with $^{15}N_2$ as feeding gas to clarify the source of NH_3. The electrolytic cell was first saturated with Ar gas to remove the contamination in the electrolyte. After that, NRR was carried out in a closed internal circulation system filled with ^{15}N (20 mL min^{-1}) at -0.7 V versus RHE for 10 h. Followed immediately, the obtained $^{15}NH_4^+$ electrolyte was acidified by 1 M H_2SO_4. Then the obtained mixture was further concentrated at 120 °C to 5 mL with the pH=2. Finally, 0.9 mL of the above electrolyte after concentration was mixed with 0.1 mL of DMSO and quantitatively determined by ^1H nuclear magnetic resonance (NMR, AVANCE III 500 MHz) with external standards. The calibration curve $^{15}NH_4^+$ solutions was created as follows. A series of $^{15}NH_4^+$ solutions with known concentrations were

prepared as standards for ^{1}H NMR measurement. The corresponding calibration curve was plotted by using the concentration of $^{15}NH_4^+$ as the x-axis and the NMR peak area as the y-axis.

Calculation of NH_3 yield, Faradaic efficiency and the NH_3 formation turn over number[3,4]

The NH_3 formation rate was determined using the following equation:

$$r(NH_3) = (c \times V) / (t \times A)$$

where c is the measured NH_3 concentration, V is the volume of the electrolyte, t is the reduction reaction time, and A is the effective area of the electrode, which is the geometric area of the electrode covering with samples.

The Faradaic efficiency was calculated as follows:

$$FE = (3F \times n \times V) / (17 \times Q)$$

where F is the Faraday constant, n is the concentration of the produced NH_3, V is the volume of the electrolyte or acid trap, t is the reduction reaction time and Q is the quantity of electric charge for one electron.

The NH_3 formation turn over number (TON) was calculated as follows:

TON = moles of NH_3 / moles of samples = NH_3 yield rate ($\mu g\, h^{-1}\, mg^{-1}_{cat}$) / (M ($NH_3$) × (1000 / M (samples)))

Density functional theory (DFT) calculation

All the calculations were carried out based on DFT methods by using the Vienna Ab initio simulation package.[5] Generalized gradient approximation (GGA) with the Perew-Burke-Ernzerhof (PBE) functional is adopted.[6] The electron-ion interaction is

described by projector augmented wave pseudopotential. The energy cutoff was set to 400 eV. The convergence threshold was 10^{-4} eV and 0.01 eV/Å for energy and force, respectively. A vacuum space of 15 Å was used to avoid the interaction between two periodic units. In order to investigate the NRR performance, the Sb trilayer and bulk were calculated in a 3×3×1 supercell. The Brillouin zone was sampled using a 5×5×1 Monkhorst-Pack k-point grid for geometry optimization and 9×9×1 for electronic properties calculations. The antimonene-edge structure was constructed with a 15 Å vacuum space along z direction and a 12 Å vacuum space along y direction to avoid the interaction due to the periodic structure.

Figure S1. The picture of Sb powders dispersed in H_2SO_4 solvent (8.0 mg mL^{-1}) with continuous stirring (400 r/min) at 298 K after 12.0 h.

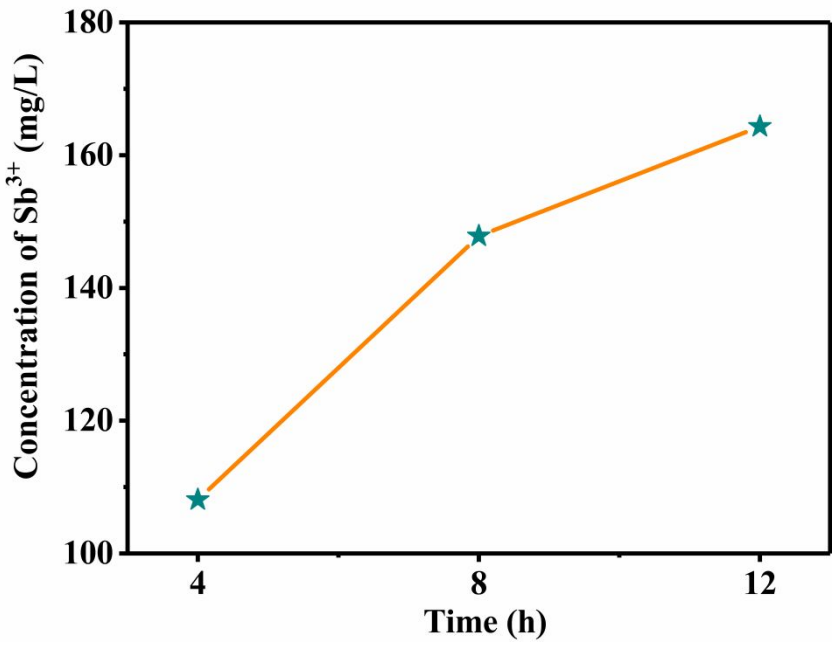

Figure S2. Concentration of Sb^{3+} at different reaction time.

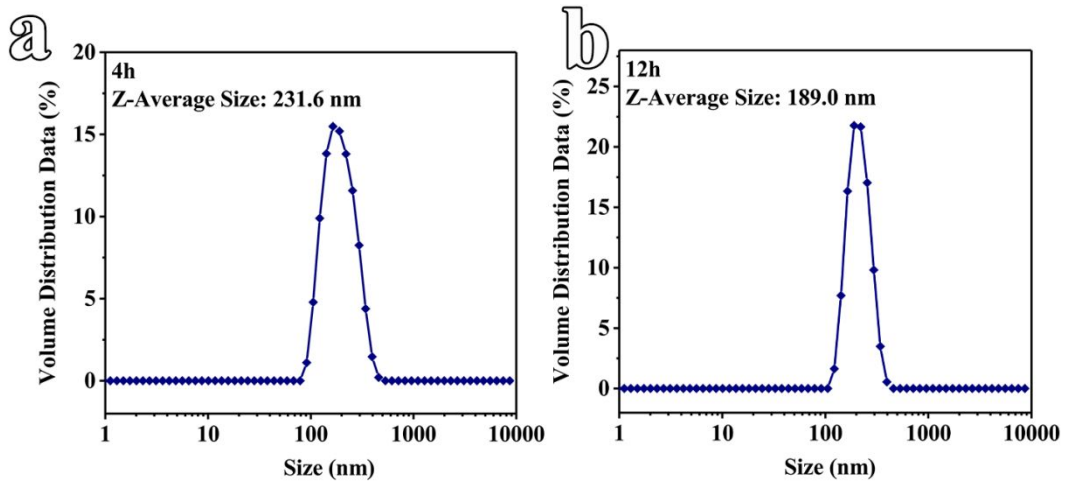

Figure S3. The particle size distribution of antimonene by the number of particles at (a) 4.0 h and (b) 12.0 h with H_2SO_4 solvent.

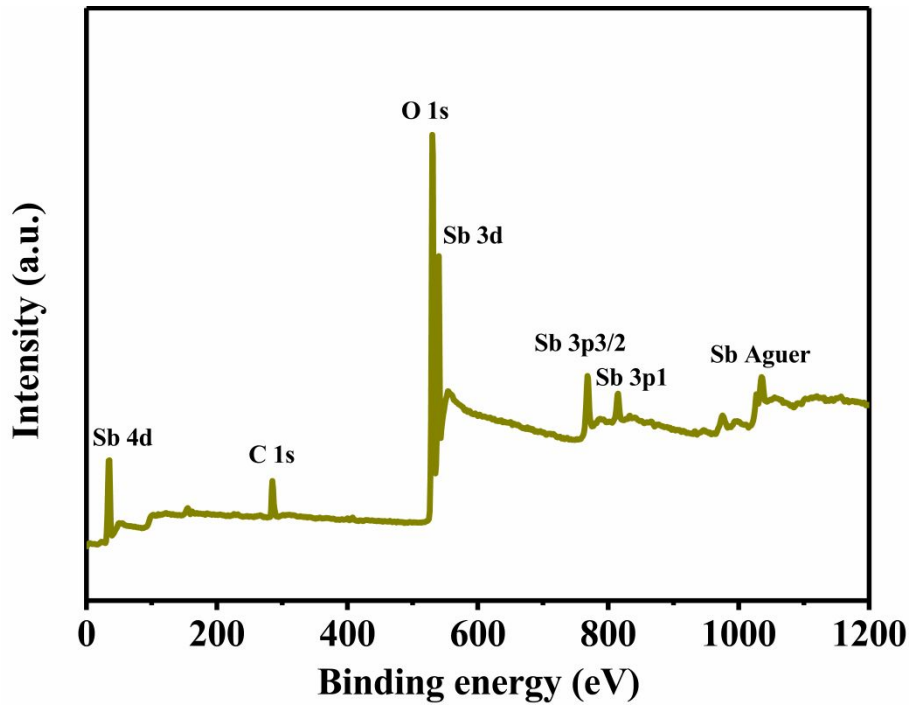

Figure S4. XPS survey spectra of antimonene.

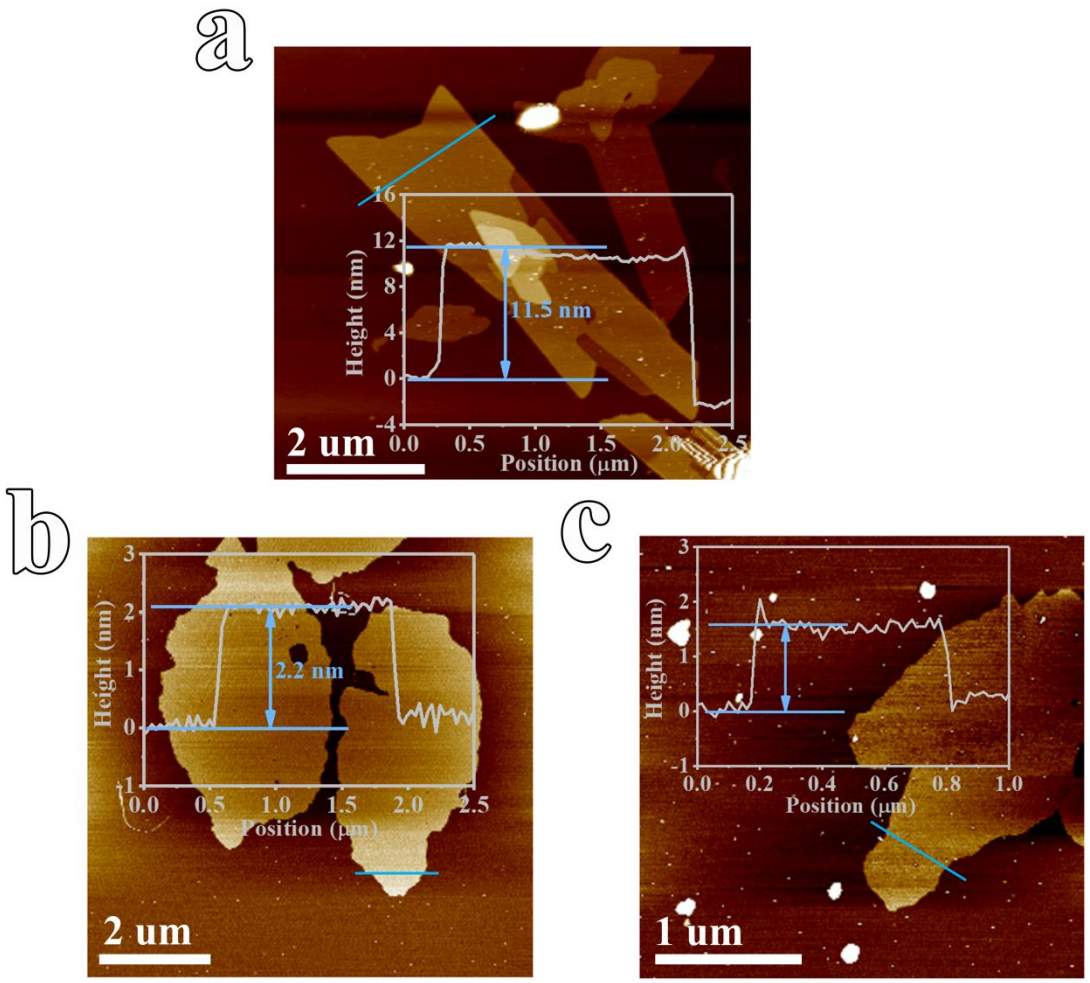

Figure S5. AFM images and measured thickness of the synthesized antimonene with varied reaction time from 4.0 to 16.0 h.

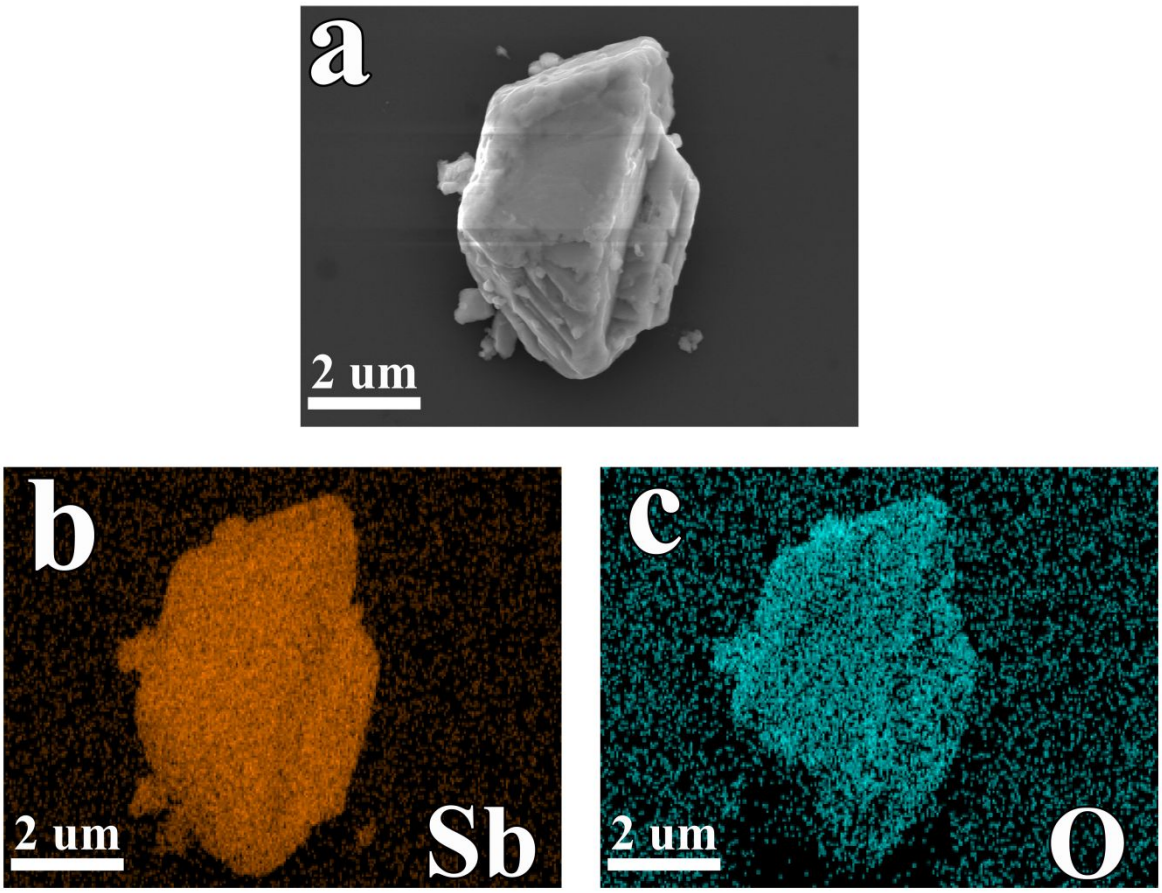

Figure S6. SEM images and corresponding EDX mapping of bulk Sb.

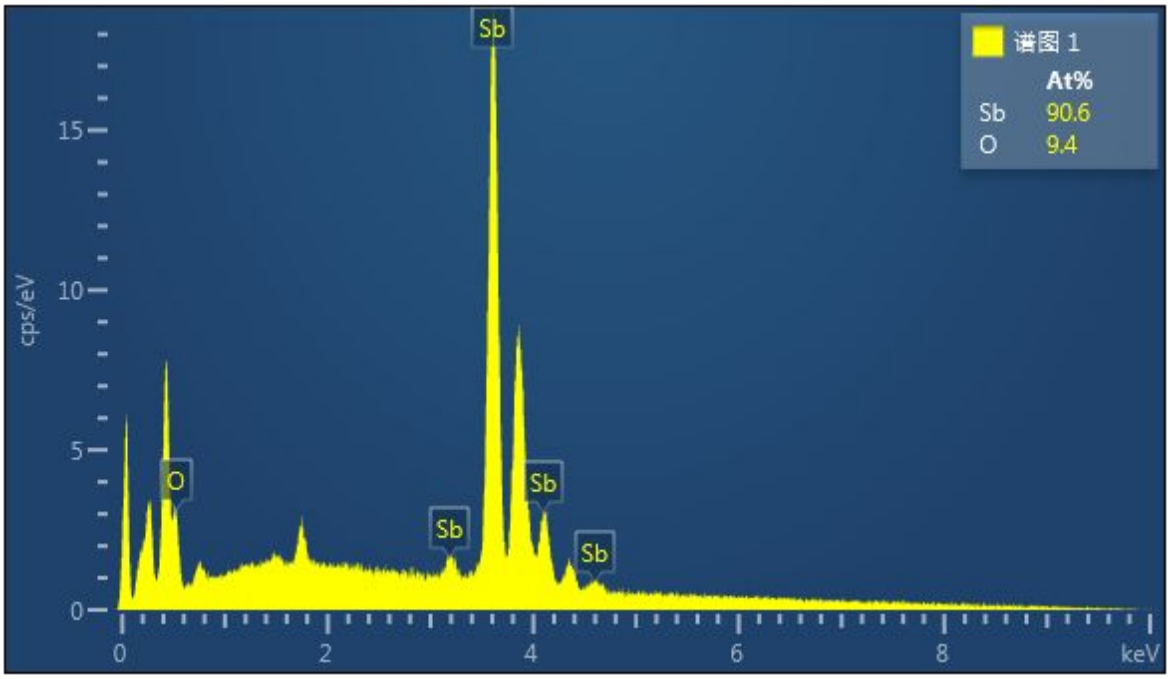

Figure S7. EDX results of bulk Sb with elements composition.

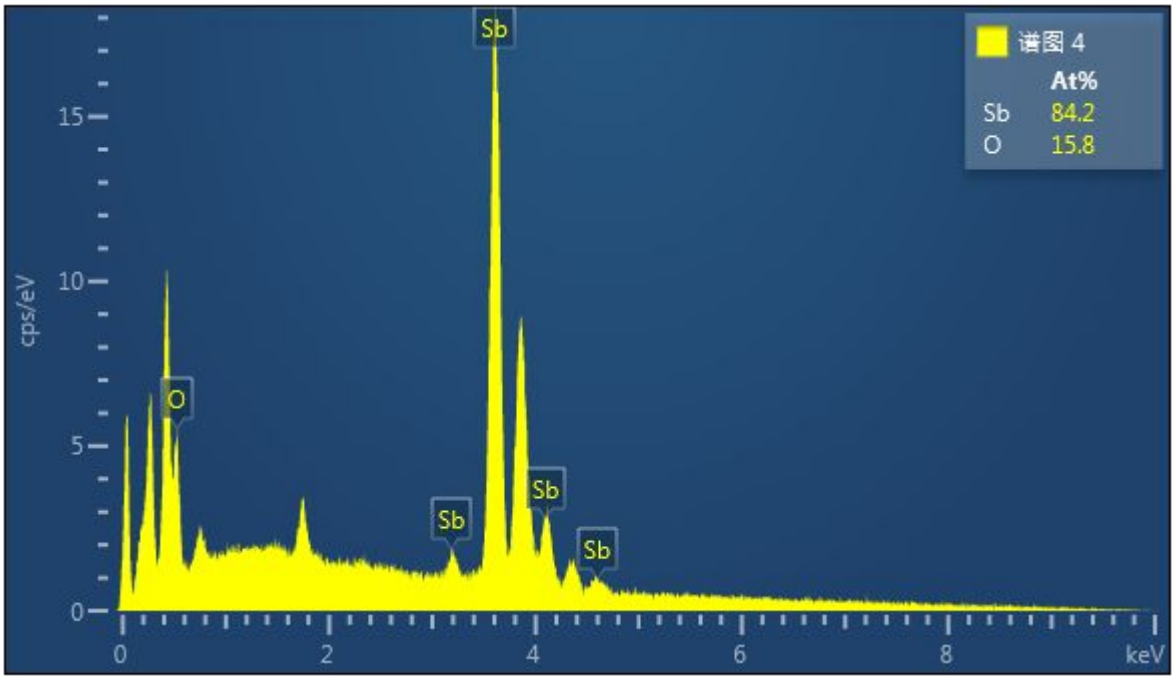

Figure S8. EDX results of antimonene with elements composition.

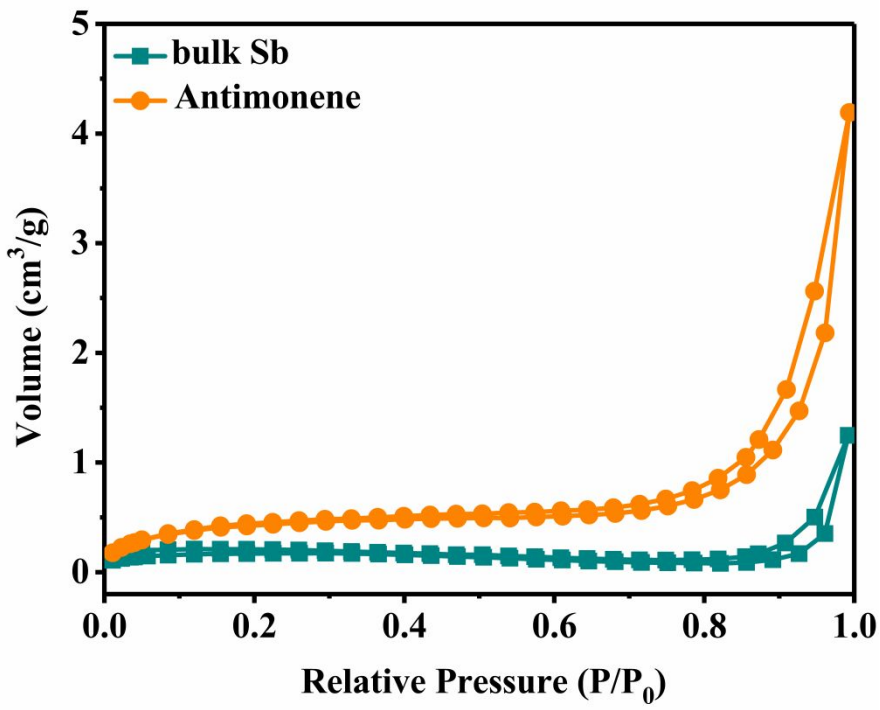

Figure S9. Nitrogen absorption-desorption isotherm of bulk Sb and antimonene.

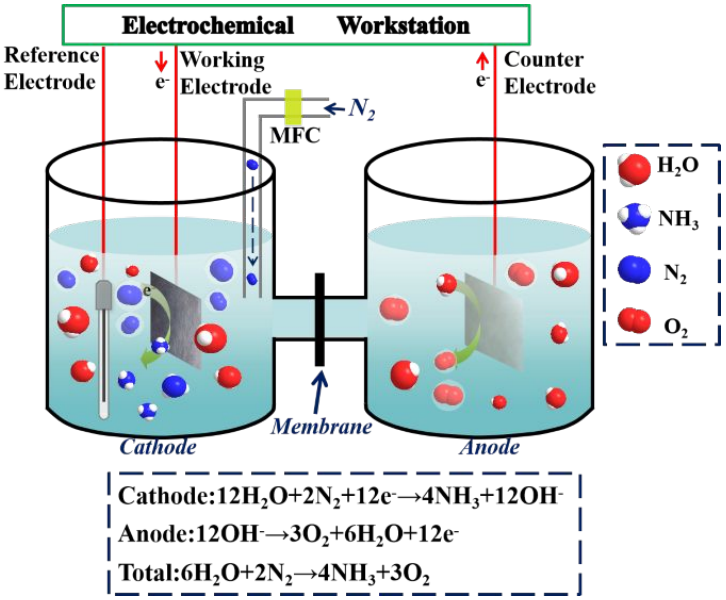

Figure S10. The schematic diagram for electrocatalytic NRR.

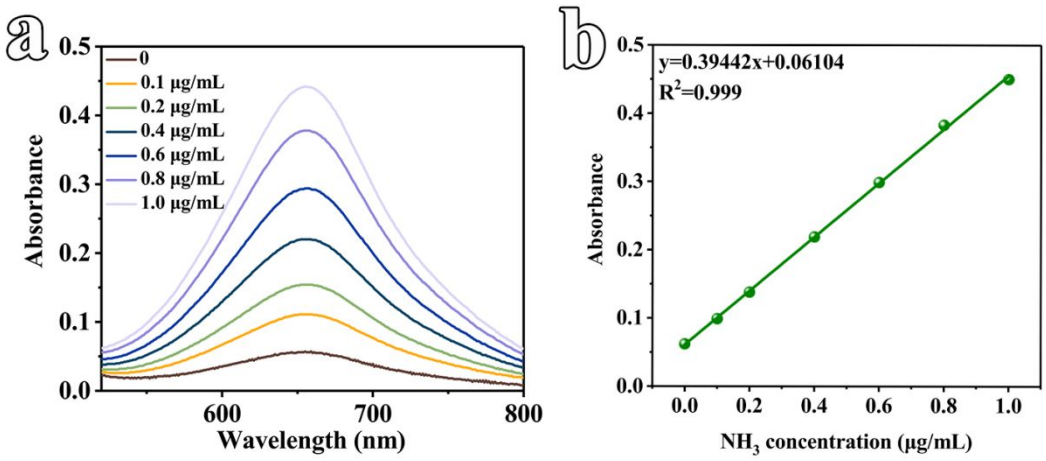

Figure S11. (a) UV-vis curves of indophenol assays after incubated for 1.0 hours. (b) A calibration curve used for estimation of NH_3 concentration.

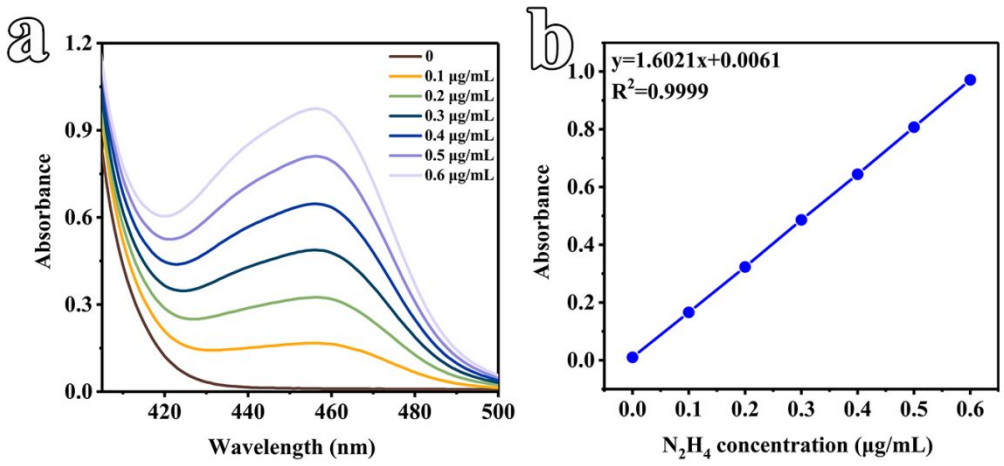

Figure S12. (a) UV-Vis curves of various concentrations of N_2H_4 stained with p-$C_9H_{11}NO$ indicator and incubated for 20 min at room temperature. (b) A calibration curve used to calculate the concentration of N_2H_4.

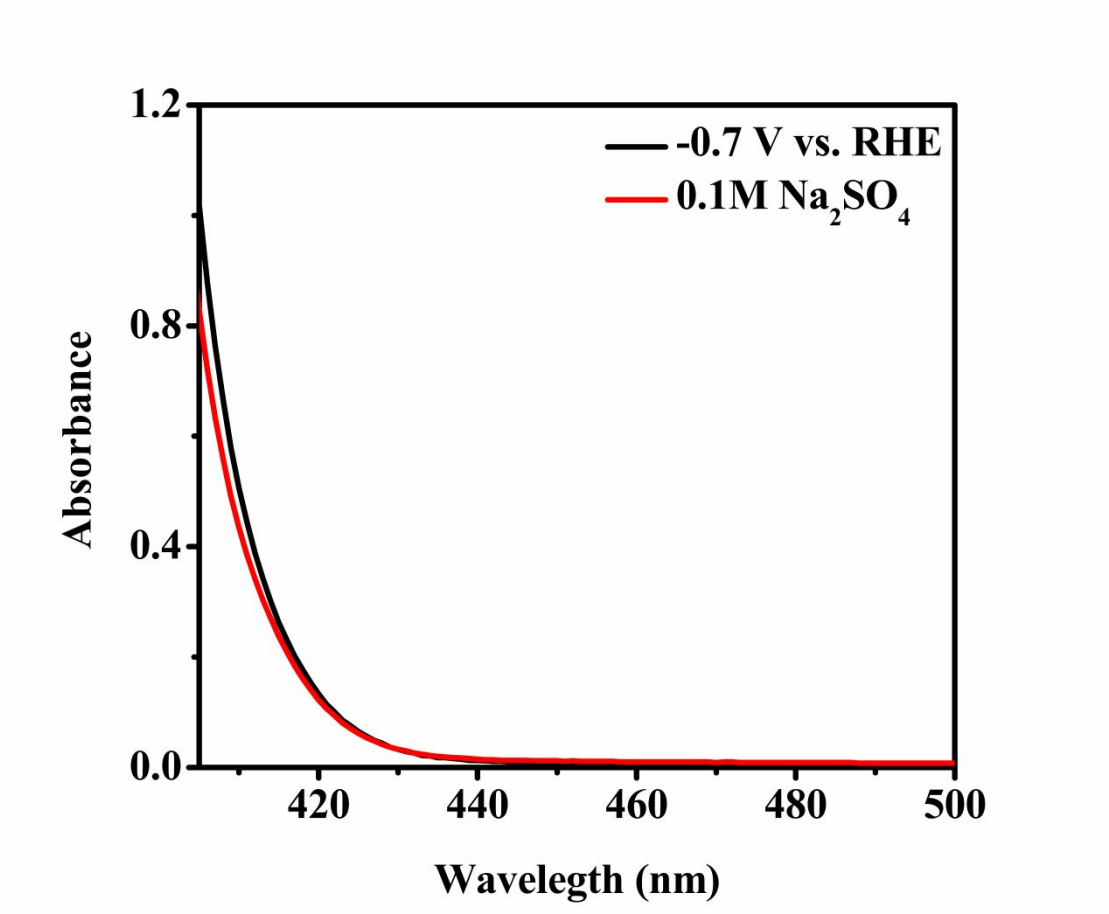

Figure S13. UV-Vis absorption spectra of the electrolytes stained with p-$C_9H_{11}NO$ indicator after NRR electrolysis at -0.7 V versus RHE at N_2 atmosphere.

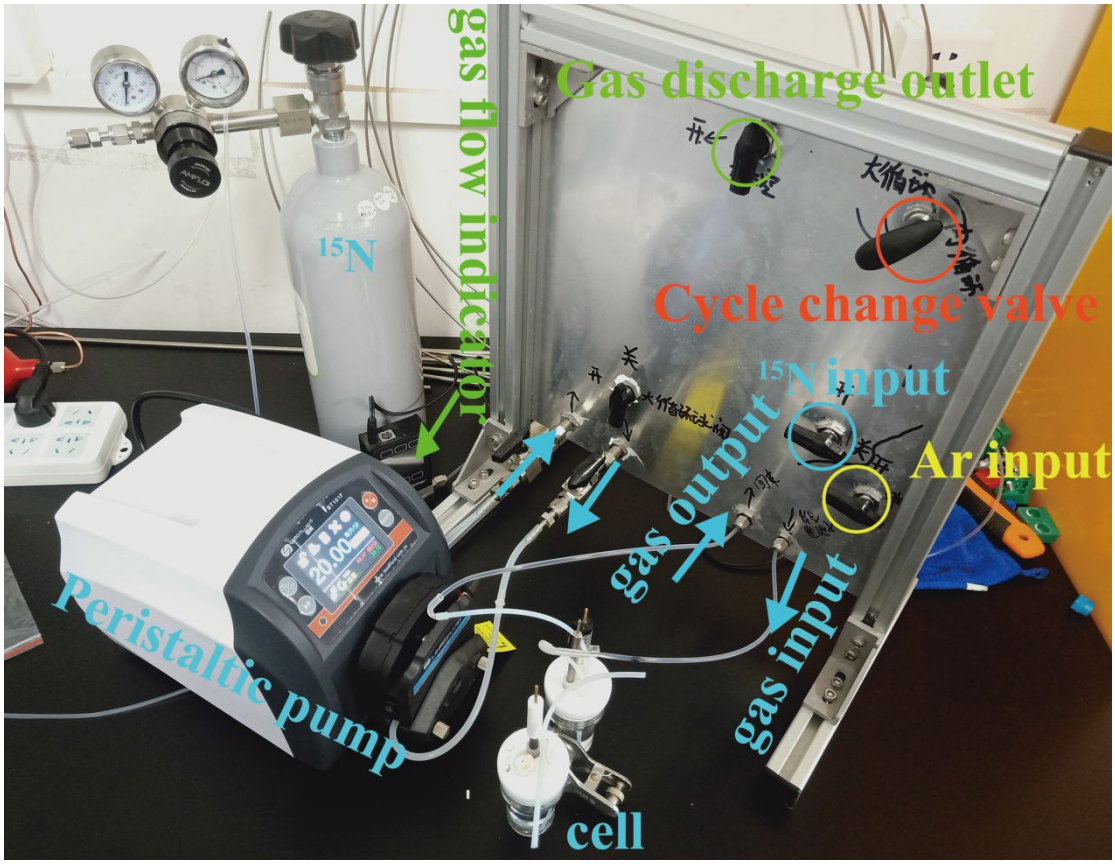

Figure S14. Schematic diagram of the reaction device.

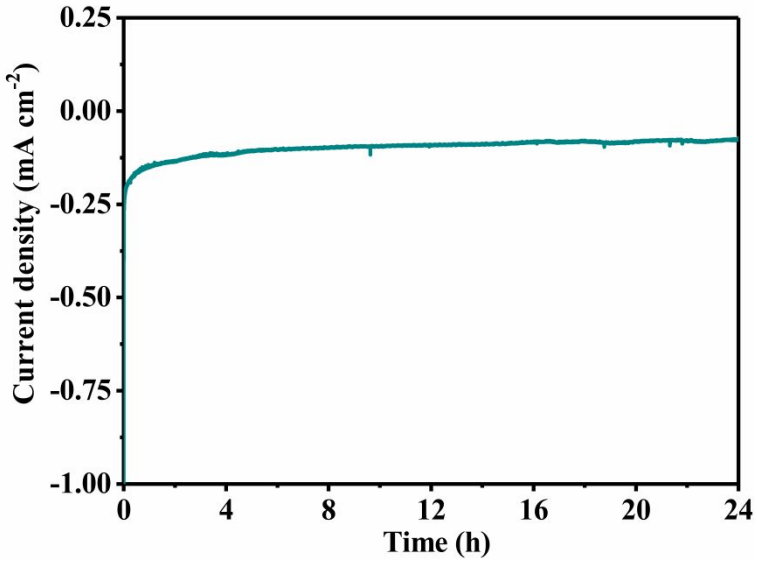

Figure S15. Chrono-amperometry results for the electrode with antimonene during electrolysis at -0.7 V versus RHE.

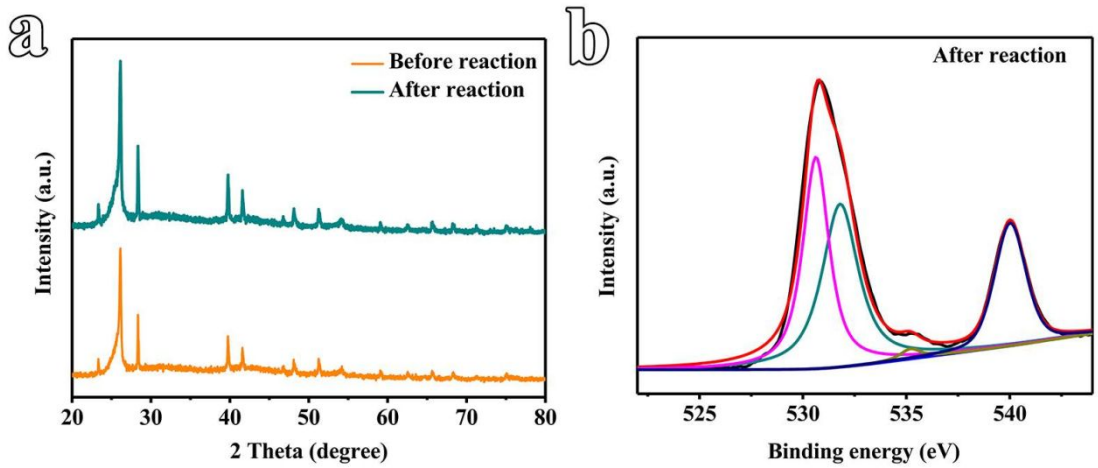

Figure S16. (a) XRD spectra of antimonene before and after NRR. (b) XPS spectra of antimonene after NRR.

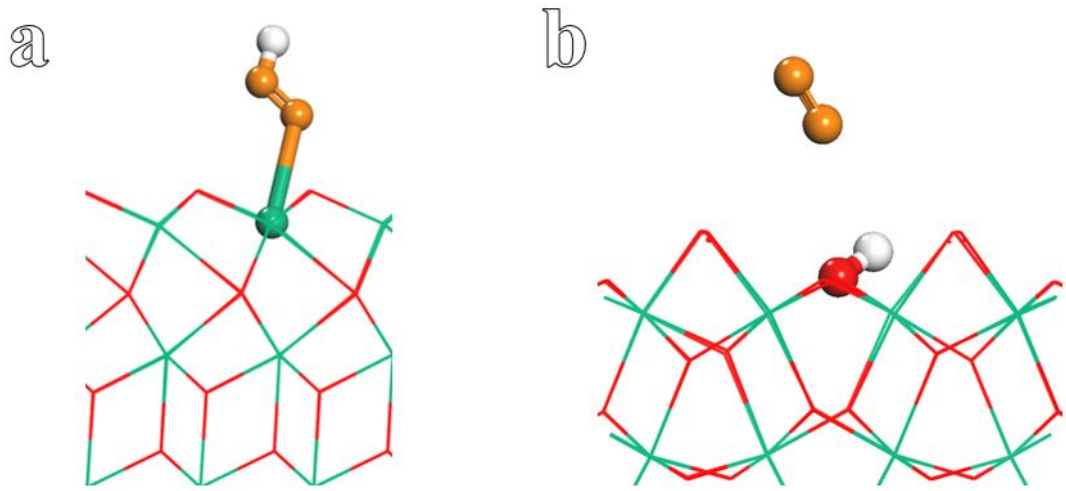

Figure S17. Schematic diagram of *N_2H configurations on (a) Sb_2O_3 nanosheets and (b) Sb_2O_5 nanosheets.

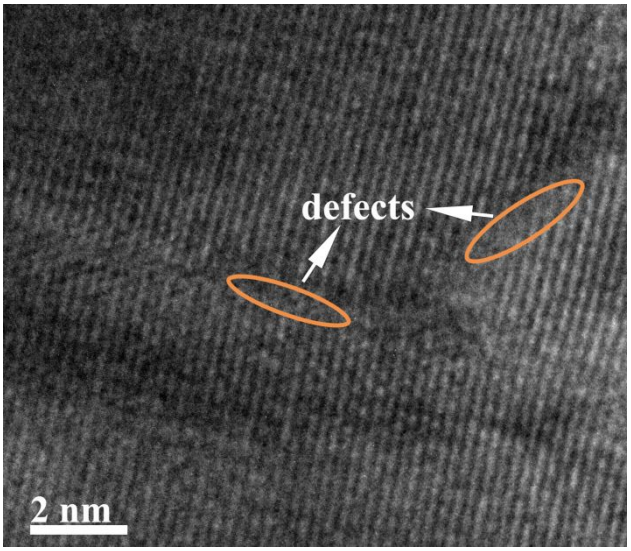

Figure S18. HRTEM image of antimonene after NRR.

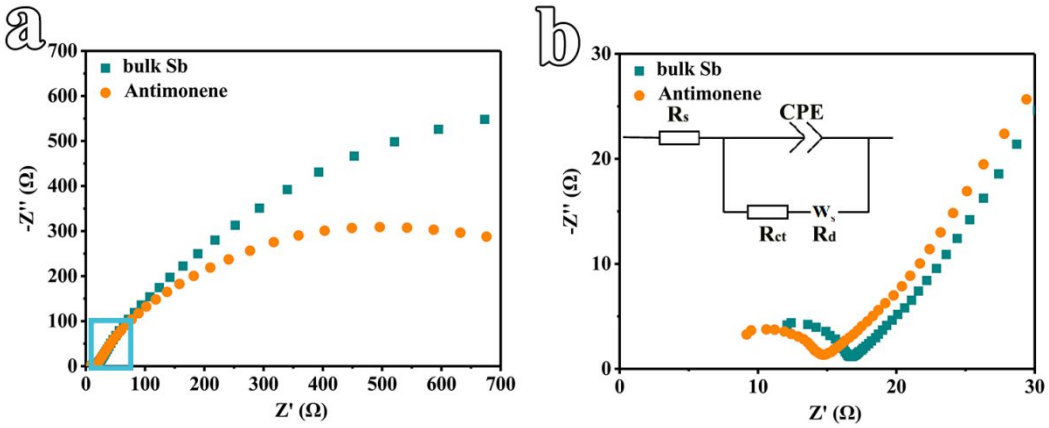

Figure S19. (a) Electrochemical impedance spectra (EIS) of bulk Sb and antimonene (8.0 h). (b) The EIS curves at high frequencies and the equivalent circuits used to fit the EIS curves (inset).

Table S1. Summary of the binding energies of the different XPS regions deconvolution for bulk Sb and antimonene at different reaction time with H_2SO_4.

		Position	%Conc.
Bulk Sb	Sb	527.92 ($4d_{5/2}$)	15.51
		537.30 ($3d_{3/2}$)	14.46
	Sb_2O_5	531.83 ($3d_{3/2}$)	26.30
	Sb_2O_3	530.28 ($4d_{5/2}$)	21.85
		539.66 ($3d_{3/2}$)	21.88
Antimonene (4h)	Sb	527.96 ($4d_{5/2}$)	14.51
		537.36 ($3d_{3/2}$)	14.77
	Sb_2O_5	531.90 ($3d_{3/2}$)	27.40
	Sb_2O_3	530.03 ($4d_{5/2}$)	22.77
		539.39 ($3d_{3/2}$)	20.55
Antimonene (8h)	Sb	528.00 ($4d_{5/2}$)	12.87
		537.39 ($3d_{3/2}$)	12.41
	Sb_2O_5	531.91 ($3d_{3/2}$)	35.60
	Sb_2O_3	530.21 ($4d_{5/2}$)	19.53
		539.60 ($3d_{3/2}$)	19.59

Table S2. Comparison of the NRR electrocatalytic activity of antimonene and other catalysts at ambient condition.

Catalyst	Electrolyte	NH_3 Yield Rate	FE	Reference
Antimonene	0.1 M Na_2SO_4	2.08 μg h^{-1} cm^{-2}	14.25%	This work
MoS_2/CFC	0.1 M Na_2SO_4	4.95 μg h^{-1} cm^{-2}	1.17%	7
	0.1 M HCl	5.19 μg h^{-1} cm^{-2}	0.096%	
Fe_2O_3-CNT	2.0 M Na_2HCO_3	0.22 μg h^{-1} cm^{-2}	0.15%	8
FeS@MoS_2/CFC	0.1 M HCl	8.75 μg h^{-1} cm^{-2}	0.22%	9
Mo nanofilm	0.01 M H_2SO_4	1.89 μg h^{-1} cm^{-2}	0.72%	10
Au nanorods	0.1 M KOH	1.65 μg h^{-1} cm^{-2}	3.88%	11
Bi NS	0.1 M Na_2SO_4	2.54±0.16 μg	10.46±1.4	12
		cm^{-2} h^{-1}	5%	
B/Graphene	0.05 M H_2SO_4	9.8 μg h^{-1} cm^{-2}	10.8%	13
AuHNCs	0.5 M $LiClO_4$	3.9 μg h^{-1} cm^{-2}	30.2%	14

Table S3. The bond length and bader charge for N_2H adsorbed on bulk Sb, Sb nanosheets and Sb_2O_3 nanosheets.

	bulk Sb	Sb nanosheets	Sb_2O_3 nanosheets
Bond length (Å)	2.72	2.44	2.81
Bader charge	-0.22	-0.45	0.03

References

[1] Zhu, D.; Zhang, L.; Ruther, R.-E.; Hamers, R.-J. Photo-Illuminated Diamond as a Solid-State Source of Solvated Electrons in Water for Nitrogen Reduction. *Nat. Mater.* **2013**, 12, 836-841.

[2] Watt, G.W.; Chrisp, J.D. Spectrophotometric Method for Determination of Hydrazine. *Anal. Chem.* **1952**, 24, 2006-2008.

[3] Han, Z.; Choi, C.; Hong, S.; Wu, T.-S.; Soo, Y.-L.; Jung, Y.; Qiu, J.; Sun, Z. Activated TiO_2 with Tuned Vacancy for Efficient Electrochemical Nitrogen Reduction. *Appl. Catal. B-Environ.* **2019**, 257, 117896.

[4] Liu, Y.-T.; Li, D.; Yu, J.; Ding, B. Stable Confinement of Black Phosphorus Quantum Dots on Black Tin Oxide Nanotubes: a Robust, Double-Active Electrocatalyst Toward Efficient Nitrogen Fixation. *Angew. Chem. Int. Ed.* **2019**, 131, 16591-16596.

[5] Kresse, G.; Hafner, J. Ab Initio Molecular-Dynamics Simulation of the Liquid-Metal-Amorphous-Semiconductor Transition in Germanium. *Phys. Rev. B* **1994**, 49, 14251-14269.

[6] Perdew, J.-P.; Burke, K.; Ernzerhof, M. Generalized Gradient Approximation Made Simple. *Phys. Rev. Lett.* **1996**, 77, 3865-3868.

[7] Zhang, L.; Ji, X.; Ren, X.; Ma, Y.; Shi, X.; Tian, Z.; Asiri, A.M.; Chen, L.; Tang, B.; Sun, X. Electrochemical Ammonia Synthesis via Nitrogen Reduction Reaction on a MoS_2 Catalyst: Theoretical and Experimental Studies. *Adv. Mater.* **2018**, 30, 1800191.

[8] Chen, S.; Perathoner, S.; Ampelli, C.; Mebrahtu, C.; Su, D.; Centi, G. Electrocatalytic Synthesis of Ammonia at Room Temperature and Atmospheric Pressure from Water and Nitrogen on a Carbon-Nanotube-Based Electrocatalyst. *Angew. Chem. Int. Ed.* **2017**, 56, 2699-2703.

[9] Guo, Y.; Yao, Z.; Timmer, B.J.; Sheng, X.; Fan, L.; Li, Y.; Zhang, F.; Sun, L. Boosting Nitrogen Reduction Reaction by Bio-Inspired FeMoS Containing Hybrid Electrocatalyst over a Wide pH Range. *Nano Energy* **2019**, 62, 282-288.

[10] Yang, D.; Chen, T.; Wang, Z. Electrochemical Reduction of Aqueous Nitrogen (N_2) at a Low Overpotential on (110)-Oriented Mo Nanofilm. *J. Mater. Chem. A* **2017**, 5, 18967-18971.

[11] Bao, D.; Zhang, Q.; Meng, F.-L.; Zhong, H.-X.; Shi, M.-M.; Zhang, Y.; Yan, J.-M.; Jiang, Q.; Zhang, X.-B. Electrochemical Reduction of N_2 under Ambient Conditions for Artificial N_2 Fixation and Renewable Energy Storage Using N_2/NH_3 Cycle. *Adv. Mater.* **2017**, 29, 1604799.

[12] Li, L.; Tang, C.; Xia, B.; Jin, H.; Zheng, Y.; Qiao, S.-Z. Two-Dimensional Mosaic Bismuth Nanosheets for Highly Selective Ambient Electrocatalytic Nitrogen Reduction. *ACS Catal.* **2019**, 9, 2902-2908.

[13] Yu, X.; Han, P.; Wei, Z.; Huang, L.; Gu, Z.; Peng, S.; Ma, J.; Zheng, G. Boron-Doped Graphene for Electrocatalytic N_2 Reduction. *Joule* **2018**, 2, 1610-1622.

[14] Nazemi, M.; Panikkanvalappil, S.R.; El-Sayed, M.A. Enhancing the Rate of Electrochemical Nitrogen Reduction Reaction for Ammonia Synthesis under

Ambient Conditions Using Hollow Gold Nanocages. *Nano Energy* **2018**, 49, 316-323.